Langmuir

Article

pubs.acs.org/Langmuir

AgAu Bimetallic Janus Nanoparticles and Their Electrocatalytic Activity for Oxygen Reduction in Alkaline Media

Yang Song, Ke Liu, and Shaowei Chen*

Department of Chemistry and Biochemistry, University of California—Santa Cruz, 1156 High Street, Santa Cruz, California 95064, United States

Supporting Information

ABSTRACT: Bimetallic AgAu Janus nanoparticles were prepared by galvanic exchange reactions of 1-hexanethiolate-passivated silver (AgC6) nanoparticles with gold(I)-mercapto-propanediol complex. The AgC6 nanoparticles were deposited onto a solid substrate surface by the Langmuir−Blodgett method such that the galvanic exchange reactions were limited to the top face of the nanoparticles that was in direct contact with the gold(I) complex solution. The resulting nanoparticles exhibited an asymmetrical distribution not only of the organic capping ligands on the nanoparticle surface but also of the metal elements in the nanoparticle cores, in contrast to the bulk-exchange counterparts where these distributions were homogeneous within the nanoparticles, as manifested in contact angle, UV−vis, XPS, and TEM measurements. More interestingly, despite a minimal loading of Au onto the Ag nanoparticles, the bimetallic AgAu nanoparticles exhibited enhanced electrocatalytic activity in oxygen reduction reactions, as compared to the monometal AgC6 nanoparticles. Additionally, the electrocatalytic performance of the Janus nanoparticles was markedly better than the bulk-exchange ones, suggesting that the segregated distribution of the polar ligands from the apolar ones might further facilitate charge transfer from Ag to Au in the nanoparticle cores, leading to additional improvement of the adsorption and reduction of oxygen.

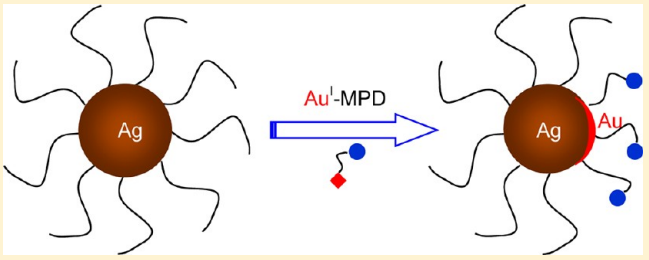

INTRODUCTION

Janus nanoparticles with two distinctly different chemical hemispheres represent a new class of nanomaterials that behave analogously to conventional surfactants and may be exploited for controlled assembly as well as directional functionalization.[1] Whereas the majority of research has thus far been focused on polymer-based Janus particles that may be up to the micrometer scale,[2] recently several effective strategies have been developed in our laboratory for the preparation of much smaller, nanometer-sized transition-metal Janus particles with hydrophobic characters on one face and hydrophilic on the other.[3] In these studies, alkanethiolate-passivated nanoparticles are used as the initial starting materials. A compact monolayer is then formed at the air|water interface or deposited onto a solid substrate surface by the Langmuir methods, and ligand exchange reactions with hydrophilic mercapto derivatives in the water subphase or in a solution medium are initiated for the replacement of the original hydrophobic ligands by the hydrophilic ones on one side of the nanoparticles, leading to the generation of amphiphilic Janus nanoparticles. It should be noted that in these earlier studies,[3] the metal cores remain unchanged. Thus, an immediate question arises. Is it possible to concurrently convert the monometallic cores into bimetallic ones with also an asymmetrical distribution of the metal elements? This is the primary motivation of the present study.

One may note that bimetallic nanoparticles are typically prepared by using two metal precursors that are reduced simultaneously forming bimetallic alloy cores. Of these, monolayer-protected alloy clusters are early examples of bimetallic nanoparticles that can be stably isolated in dry form.[4] The metal compositions in and on the core surface may differ significantly from the initial feed ratio of metal salts used in nanoparticle synthesis. Another common procedure involves the deposition of a second metal onto the surface of preformed nanoparticles and hence the production of core−shell nanoparticles where the thickness of the second metal layer in principle may be controlled by varied experimental parameters.[5] Alternatively, galvanic exchange reactions have also been used to (partly or fully) replace the metal elements of the original nanoparticles forming new functional nanostructures of controlled metal compositions. Such reactions have, for example, been employed to replace Cu or Ag particles encapsulated in dendrimers by more noble metals (e.g., Au, Pt, and Pd) and to prepare bi- and trimetallic nanoparticles.[6] Galvanic displacement reactions have also been used to prepare the bimetallic sulfides of PbCd and ZnCd, CoPt core−shell bimetallic nanoparticles, AuAg, PdAg, AuPd, and AuCu bimetallic alloy nanoparticles, etc.[7] This is to take advantage of the different redox potentials of varied metal/ion couples where ions of more noble metals may be reduced by the less

Received: August 30, 2012
Revised: November 14, 2012
Published: November 19, 2012

 © 2012 American Chemical Society

Scheme 1. Schematic for the Preparation of Bimetallic Janus Nanoparticles Based on Interfacial Galvanic Exchange Reactions of AgC6 Nanoparticles with Au^{I}-MPD Complex

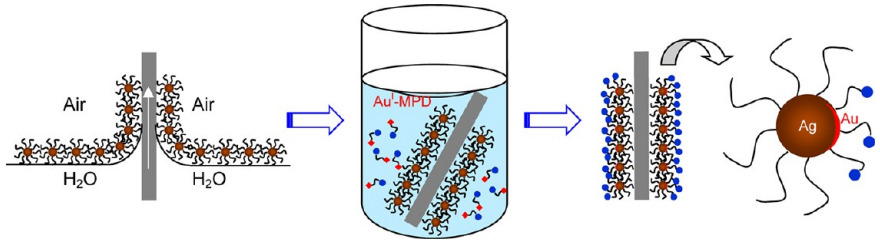

noble metal elements. It should be noted that in these early reports the two metal elements are presumed to be distributed homogeneously within the nanoparticles as the reactions take place in a single solution phase. Importantly, the introduction of a new metal element in the cores leads to an apparent variation of both the physical and chemical properties of the resulting nanoparticles, which may be exploited, for instance, for optical, electronic, as well as (electro)catalytic applications.[4,7b,8] In fact, a number of catalysts for fuel cell electrochemistry are based on bimetallic nanoparticles.

It should be noted that fuel cells have been recognized as a promising clean and efficient power source for diverse applications. Of these, alkaline fuel cells (AFCs) have gained a great deal of attention because alkaline media provide a less corrosive environment to the catalysts and electrodes,[9] the kinetics of oxygen reduction reactions (ORR) is more rapid in alkaline electrolytes than in acidic ones, and the chemical energy stored in small molecule fuels (such as hydrogen, hydrazine, and alcohols)[10] and oxidants (oxygen) can be directly and efficiently converted into electricity, rendering AFCs a promising power supply for portable electronics. In AFCs, Ag-based catalysts have been examined as a substitute of Pt because of their obviously low costs and high stability in alkaline media; yet, typically a large amount of silver is required because of its relatively low catalytic activity. In recent years, a number of strategies have been proposed and employed to improve the ORR activity of Ag nanoparticles that typically involve manipulation of the elemental composition, size, and surface atomic arrangements of the nanoparticle catalysts. Among these, Ag-based alloy catalysts show significantly enhanced ORR activity as compared with pure Ag.[11]

In the present study, we take advantage of the Langmuir methods as well as galvanic exchange reactions to prepare bimetallic nanosized AgAu Janus particles. Specifically, 1-hexanethiolate-passivated silver (AgC6) nanoparticles were used as the starting materials. A monolayer was deposited onto a glass slide surface by the Langmuir−Blodgett method, which was then immersed into a solution of gold(I)-mercaptopropanediol (Au^{I}-MPD) complex. Galvanic exchange reactions between the AgC6 nanoparticles and Au^{I}-MPD led to the displacement of part of the Ag atoms on the nanoparticle cores with Au and concurrently the replacement of the original hydrophobic hexanethiolates with the more hydrophilic MPD ligands. Note that the reactions were restricted to the side of the nanoparticles that was in direct contact with the solution because of surface ligand intercalation between neighboring particles that impeded the accessibility of the bottom face to the solution ligands. The asymmetrical chemical structures of the resulting nanoparticles were characterized by a variety of spectroscopic measurements. Interestingly, the bimetallic Janus nanoparticles exhibited enhanced electrocatalytic activity in ORR as compared with the original monometallic Ag nanoparticles or the bimetallic nanoparticles that were prepared in a single phase (the so-called bulk-exchange particles), suggesting that interfacial engineering is key to the manipulation and optimization of the nanoparticle electronic properties and hence the interactions with oxygen and ultimately the ORR performance.

EXPERIMENTAL SECTION

Chemicals. Silver nitrate ($AgNO_3$, Fisher Scientific), sodium borohydride ($NaBH_4$, ≥98%, ACROS), tetra-*n*-octylammonium bromide (TOABr, 98%, ACROS), 1-hexanethiol (C6SH, 96%, ACROS), and 3-mercaptopropane-1,2-diol (MPD, Aldrich, 95%) were all used as received without any further purification. Solvents were purchased at the highest purity available from typical commercial sources and also used as received. Hydrogen tetrachloroauric acid ($HAuCl_4{\cdot}xH_2O$) was synthesized by dissolving ultrahigh purity gold (99.999%, Johnson Matthey) in freshly prepared aqua regia followed by a crystallization process.[12] Water was deionized with a Barnstead Nanopure water system (18.3 MΩ cm).

The Au^{I}-MPD complex was prepared by mixing a stoichiometric amount of $HAuCl_4$ and MPD in methanol, which was a white precipitate as a result of the reduction of Au^{III} to Au^{I} by the thiol moieties. The precipitate was collected by centrifugation and washed extensively with methanol.

Synthesis of AgC6 Nanoparticles. 1-Hexanethiolate-passivated silver nanoparticles were prepared by following the Brust method.[13] Experimentally, 30 mL of an aqueous $AgNO_3$ solution (0.03 M) was mixed with 20 mL of a toluene solution of TOABr (0.20 M) and stirred vigorously for 1 h. The gray organic phase was collected, into which 150 μL of 1-hexanethiol was added with a Hamilton microliter syringe. After the solution was stirred for 15 min, 24 mL of a freshly prepared ice-cold aqueous solution of 0.43 M $NaBH_4$ was added dropwise, and the solution color turned dark brown immediately, signifying the formation of silver nanoparticles. The reaction mixture was stirred for 4 h before the organic phase was collected and washed five times with methanol to remove the phase transfer catalysts, excessive 1-hexanethiol, and reaction byproducts. The resulting silver nanoparticles were denoted as AgC6.

Preparation of AgAu Bimetallic Janus Nanoparticles. AgAu bimetallic Janus nanoparticles were prepared by interfacial galvanic exchange reactions of AgC6 nanoparticles with Au^{I}-MPD complex. The procedure is depicted in Scheme 1, similar to that used previously in the preparation of monometallic Janus nanoparticles.[3b] First, a monolayer of the AgC6 nanoparticles was deposited by the Langmuir−Blodgett method onto a clean glass slide surface at a sufficiently high surface pressure where ligand intercalation between neighboring nanoparticles occurred (step i). The surface area of the glass slide was typically 8 cm × 3 cm. The glass substrate with the particle monolayer was then immersed into a water/methanol (v/v = 1:1) solution of the Au^{I}-MPD complex at a concentration of ca. 0.25 mg/mL (step ii). The galvanic exchange reactions of the AgC6 particles with the Au^{I}-MPD complex took place only at the top face of the particles that was in direct contact with the water/methanol phase, leading to the generation of Janus nanoparticles (step iii). At varied immersion time intervals, the glass slide was taken out of the Au^{I}-MPD

dx.doi.org/10.1021/la303513x | *Langmuir* 2012, 28, 17143−17152

solution, gently rinsed with copious amounts of methanol and water to remove excessive Au^I-MPD, displaced silver ion, and hexanethiolate ligands, dried in a gentle stream of ultrahigh-purity nitrogen, and then subject to contact angle measurements (see below) before being collected into a vial by THF. At least four batches of particle samples were prepared and collected under identical conditions so that there were enough materials for further analyses. The resulting Janus particles were found to be soluble in chloroform and THF.

As a control measurement, galvanic exchange reactions of the AgC6 nanoparticles with Au^I-MPD were also carried out by mixing a calculated amount of AgC6 nanoparticles and Au^I-MPD ligands in THF and were stirred for varied periods of time. The solution was then dried under reduced pressure with a rotary evaporator, and excessive ligands were removed by extensive rinsing with methanol. The resulting particles were denoted as bulk-exchange particles and, similar to the Janus nanoparticles, were also soluble in chloroform and THF.

Characterizations. Contact angles were measured with a Tantec CAM-PLUS contact angle meter. For each sample, at least eight independent measurements were carried out for statistical analyses. The UV–vis spectra were collected with a UNICAM ATI UV4 spectrometer at a particle concentration of ca. 0.5 mg/mL in THF using a 1 cm quartz cuvette. The optical properties of the bulk-exchange nanoparticles were monitored at various reaction times. X-ray photoelectron (XPS) spectra were recorded with a PHI 5400/XPS instrument equipped with an Al Kα source operated at 350 W and 10^{-9} Torr. Silicon wafers were sputtered by argon ions to remove carbon from the background and used as substrates.

Transmission Electron Microscopy (TEM). The morphology and sizes of the nanoparticles were characterized by transmission electron microscopic studies (TEM, Philips CM300 at 300 kV). At least 200 nanoparticles were measured to obtain a size histogram. Energy-dispersive X-ray spectroscopy studies (EDS) were carried by using a Philips CM200/FEG transmission electron microscope.

Electrochemistry. The electrochemical setup consists of a CHI710 electrochemical workstation with a Pt foil counter electrode and a reversible hydrogen electrode (RHE) at room temperature. The working electrode was a rotating ring-disk electrode (RRDE, AFE7R9GCAU from Pine Instrument Co.) with a glassy carbon disk (GC, diameter 5.61 mm) and a gold ring. The collection efficiency (N) was determined to be 37.3% by RRDE measurements in 5 mM $K_4Fe(CN)_6$ + 0.1 M $Sr(NO_3)_2$, which is consistent with the manufacturer's value of 37%.[14] The RRDE was prepared according to a procedure proposed by Gloagen et al.[15] In a typical experiment, 500 μg of the AgC6 or the bimetallic (Janus or bulk-exchange) nanoparticles were mixed with 2 mg of XC-72 carbon black (mass ratio of metal:C = 1:4) in toluene with 3 μL of a Nafion 117 solution (5 wt %) and dispersed under sonication. A measured volume (ca. 10 μL) of this catalyst ink was then transferred via a syringe onto the freshly polished glassy carbon disk. The solvent was evaporated at room temperature yielding a catalytic loading of 15 μg with ca. 3 μg of metals (20 wt.%).

RESULTS AND DISCUSSION

Previously it has been shown that galvanic exchange reactions of core metals occur when alkanethiolate-passivated metal nanoparticles mix with thiolate complexes of more noble metals in solution, forming bimetallic nanoparticles.[7b] Thus, the reactivity of AgC6 nanoparticles with Au^I-MPD was first examined by UV–vis spectroscopic measurements, as the (partial) replacement of the Ag core atoms by Au is anticipated to lead to a drastic variation of the nanoparticle optical properties. It is well-known that pure gold and silver nanoparticles exhibit distinctly defined surface plasmon resonance in the visible region at about 520 and 420 nm, respectively.[16] In fact, for the as-prepared AgC6 nanoparticles, UV–vis spectroscopic measurements showed that the surface plasmon band was centered at 422 nm, as manifested by the black curve in Figure 1. Upon the addition of the Au^I-MPD complex, core metal galvanic reactions occurred, and the

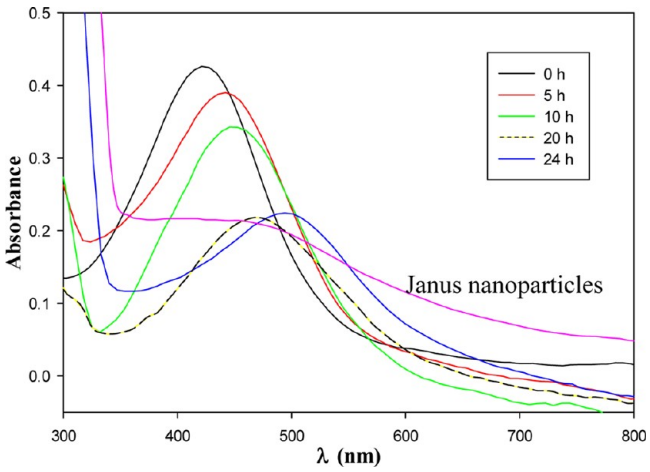

Figure 1. UV–vis spectra of AgC6 nanoparticles after galvanic exchange reactions with Au^I-MPD for varied periods of time (as specified in the figure legends). The spectrum of Janus nanoparticles was also included (magenta curve) where the nanoparticles were prepared by interfacial galvanic exchange reactions for 24 h. The concentrations of the particles were all ca. 0.5 mg/mL in THF.

surface plasmon band position was found to shift accordingly, for instance, to 442 nm after reactions for 5 h (red curve), 450 nm for 10 h (green curve), 467 nm for 20 h (dashed black/yellow curve), and 493 nm at 24 h (blue curve). Such a red-shift of the surface plasmon resonance is consistent with the fact that an increasing amount of Au was incorporated onto the silver core surface as the surface plasmon band position is sensitively dependent upon the elemental composition of the metal nanoparticles.[17] Furthermore, the appearance of a single absorption band indicates that bimetallic nanoparticles are formed rather than a simple mixture of monometallic nanoparticles. Note that similar observations have been reported by Link et al. where they synthesized a series of gold–silver alloy nanoparticles and observed a linear blue-shift of the surface plasmon peak position with increasing silver content,[18] by Mulvaney and co-workers where metallic Au was deposited onto Ag colloidal nanoparticle surfaces by chemical reduction,[5b] and by Shon et al. of galvanic exchange reactions between Ag nanoparticles and Au^I thiolate complexes.[7b]

Such unique chemistry was then exploited for the preparation of Janus nanoparticles with asymmetrical bimetallic cores by using an interfacial engineering procedure that we developed earlier (Scheme 1).[3b] Specifically, by confining the galvanic exchange reactions to only one face of the nanoparticles, it is envisaged that the resulting nanoparticles would exhibit not only a segregated distribution of the two metal elements in the core but also two faces of protecting ligands that are chemically different. As manifested in Scheme 1, a monolayer of AgC6 nanoparticles deposited onto a glass slide surface was immersed into a solution of Au^I-MPD and the galvanic exchange reactions were limited to the top face of the nanoparticles, leading to the formation of Janus nanoparticles with bimetallic cores. To confirm the amphiphilic characters of the surface protecting layers of the resulting nanoparticles, the contact angle of the nanoparticle monolayers was monitored at different immersion time intervals (step ii). The result is depicted in Figure 2. It can be seen that, prior to the immersion

dx.doi.org/10.1021/la303513x | Langmuir 2012, 28, 17143–17152

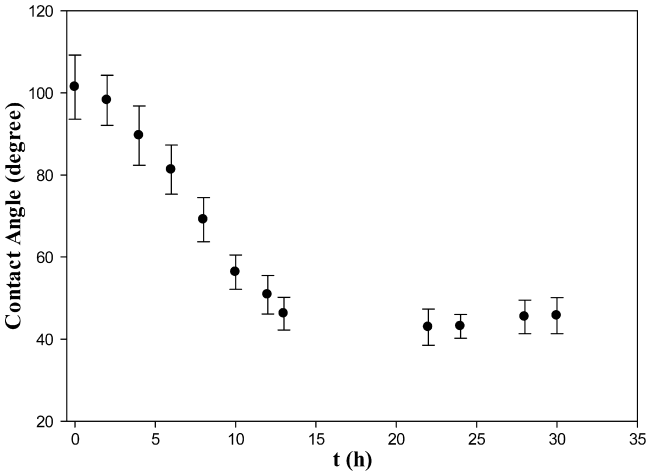

Figure 2. Contact angles of a Langmuir–Blodgett monolayer of AgC6 nanoparticles after being immersed in ca. 2.5 mg/mL Au^{I}-MPD complex in methanol/water (v:v = 1:1) at room temperature for different periods of time. Error bars reflect the standard deviations of at least eight independent measurements.

of the nanoparticle monolayers into the Au^{I}-MPD solution (i.e., at t = 0 h), the contact angle of the AgC6 nanoparticle film was 101.4 ± 7.8°, which is consistent with those observed with self-assembled monolayers of alkanethiols on silver substrate surfaces.[19] After 1 h of immersion, the contact angle decreased slightly to 98.2 ± 6.1°. Further immersion led to a more rapid decrease of the contact angle, and at t = 13 h, it dropped drastically to 46.2 ± 4.0° and remained statistically invariant thereafter (45.7 ± 4.4° at 30 h). Note that this contact angle is consistent with that of MPD self-assembled monolayers on metal surfaces.[3] These observations suggest the effective replacement of the original hydrophobic hexanethiolate ligands by the more hydrophilic MPD which reached equilibrium at around 13 h. Such a dynamic change of the contact angle of the nanoparticle monolayers with immersion time might be accounted for by the nanocrystalline morphology of the nanoparticles, where galvanic exchange reactions on alkanethiolate-protected silver nanoparticles presumably started with the surface defect sites (e.g., edges and vertices) and then propagated to the terrace sites. Similar behaviors have been observed previously in ligand exchange reactions of AuC6 nanoparticles with 2-(2-mercaptoethoxy)-ethanol (MEA)[3b] and 3,5-octadiyne-1-ol-8-thiol (DAT)[20] as the hydrophilic ligands. This indicates that while Au^{I} was reduced into Au^{0} by the Ag core atoms, the MPD ligands were also incorporated into the nanoparticle surface protecting layer. In fact, the formation of bimetallic AuAg Janus nanoparticles was also manifested in UV–vis spectroscopic measurements with a broad absorption band at around 472 nm (magenta curve in Figure 1, for the sample prepared by reactions for 24 h) that is in the intermediate range between those of pure Ag and Au nanoparticles.

In addition, experimentally, we observed no loss of nanoparticles into the water/methanol solution during the entire experimental procedure, which indicates that the galvanic replacement reactions were limited only to the top face of the AgC6 nanoparticles, as nanoparticles fully functionalized with the hydrophilic MPD ligands would have become dispersible in the reaction media of water/methanol mixed solvents. This may be ascribed to the inaccessibility of the bottom face of the nanoparticles to the Au^{I}-MPD complex because of ligand intercalation, which impeded interfacial mobility of the nanoparticles on the substrate surface and, hence, led to the formation of asymmetrically functionalized nanoparticles.

The bimetallic nature of the resulting nanoparticles was further manifested in scanning transmission electron microscopic measurements. Figure 3 depicts the representative high-resolution TEM micrographs of the (a) original AgC6, (b) bulk-exchange and (c) Janus nanoparticles. Note that the last two samples were prepared by galvanic exchange reactions of AgC6 nanoparticles with Au^{I}-MPD for 24 h. It can be seen that the nanoparticles were all very well dispersed, indicating effective protection of the nanoparticles by the mercapto ligands before and after core metal galvanic exchange reactions. Also, the nanoparticle core size remained statistically unchanged. In fact, the average core diameter was found to be 5.70 ± 0.82, 5.79 ± 1.02, and 5.36 ± 0.85 nm, for the as-prepared AgC6, bulk-exchange, and Janus particles, respectively, as depicted in the right insets to Figure 3. Furthermore, the nanoparticles all exhibited well-defined crystalline lattice fringes, as highlighted in the left insets, with a spacing of 0.235 nm that may be ascribed to the (111) planes of both fcc silver[21] and gold.[22]

As bulk gold and silver exhibit very close lattice constants (0.408 and 0.409 nm, respectively), it is challenging to detect the distribution of Au on the Ag nanoparticle surface by their lattice fringes. This can be done, however, by elemental mapping based on energy-dispersive X-ray analysis (EDS). Figure 4 shows two representative elemental maps of a (a) Janus and (b) bulk-exchange nanoparticle, with the red symbols for silver and green for gold. It can be seen that for the Janus nanoparticles in panel (a) gold can be identified only on one side of the nanoparticles whereas the silver signals are distributed all over the nanoparticles. In sharp contrast, for the bulk-exchange nanoparticle in panel (b), both the Ag and Au elements are distributed rather homogeneously throughout the entire nanoparticle.

The incorporation of Au onto the Ag nanoparticles by galvanic exchange reactions was also manifested in XPS measurements. Figure 5 shows the XPS survey spectra of the (a) Ag 3d and (b) Au 4f regions for the Janus (bottom curves) and bulk-exchange (top curves) nanoparticles. The Ag 3d electrons can be readily identified at 368.00 and 374.10 eV for the bulk-exchange nanoparticles, whereas for the Janus counterparts, the binding energies blue-shifted slightly to 368.55 and 374.20 eV; meanwhile, a small red-shift was observed of the Au 4f electrons, which appeared at 84.20 and 88.15 eV for the bulk-exchange nanoparticles and 84.05 and 87.85 eV for the Janus nanoparticles. Note that these values (Table 1) are qualitatively comparable to those reported previously for AgAu bimetallic core–shell or alloy nanoparticles;[7b,23] and more interestingly, the increase (decrease) of the binding energies of the Ag 3d (Au 4f) electrons of the Janus nanoparticles, as compared to those of the bulk-exchange counterparts, suggests that (partial) charge transfer occurred from Ag to Au. While the detailed mechanism is not clear at this point, this appears to be facilitated by the asymmetrical distribution of Au on the nanoparticle surface, as well as by the segregated distribution of the polar MPD ligands from the apolar hexanethiolates in the Janus nanoparticles (and hence the formation of an apparent dipole) that stabilized the extra electron density on the gold sites; in contrast, the ligands were distributed rather homogeneously on the bulk-exchange

dx.doi.org/10.1021/la303513x | Langmuir 2012, 28, 17143–17152

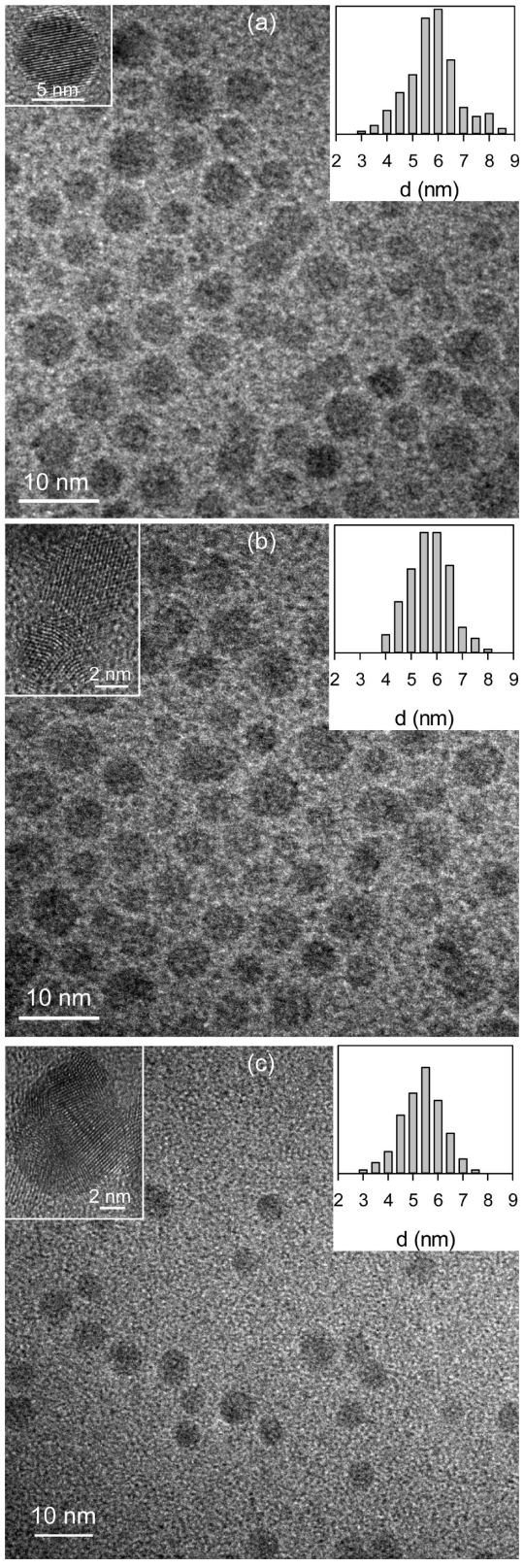

Figure 3. Representative TEM images of (a) AgC6 nanoparticles, (b) bulk-exchange, and (c) Janus nanoparticles. The last two samples were prepared by galvanic exchange reactions of AgC6 nanoparticles with Au^{I}-MPD for 24 h. The scale bars are all 10 nm. Left insets show the corresponding high-resolution TEM micrographs with the scale bars of (a) 5 nm and (b and c) 2 nm. Right insets are the respective core size histograms.

nanoparticle surface and hence the nanoparticles carried zero dipole. Such a unique property of the Janus nanoparticles may be exploited for further improving the electrocatalytic activity of the nanoparticles in oxygen reduction, as manifested below.

Furthermore, from the XPS measurements (Figure 5), the Au/Ag atomic ratio can be quantified. For Janus nanoparticle, the Au/Ag ratio was estimated to be 1:21.9, and a somewhat greater ratio was observed of the bulk-exchange particles at 1:16.3. Note that, based on the nanoparticle core diameters as determined by TEM measurements (Figure 3), the surface atoms constitute about 25% of the total atoms of the metal cores of these nanoparticles.[24] This means that, in the preparation of the Janus nanoparticles, approximately 17% of the Ag atoms (and the associated hexanethiolate ligands) in the surface layer was replaced by Au (and MPD ligands), and 23% for the bulk-exchange nanoparticles. This change of the nanoparticle surface structures (and composition) is consistent with the UV−vis measurements in Figure 1 and the contact angles reported in Figure 2. Previously it was observed[25] that, for an alkanethiol monolayer self-assembled on Au(111) thin films, the contact angle was about 112°, which decreased drastically to only 45° when 25% of the ligands were replaced by hydroxyl-terminated thiol molecules. In the present study, the contact angle was found to decrease from about 101° for a monolayer of the as-prepared AgC6 nanoparticles to 46° after galvanic exchange reactions with Au^{I}-MPD for 24 h (forming the aforementioned Janus nanoparticles, Figure 2).

The nanoparticles prepared above were then used for the electrocatalytic reduction of oxygen, a critical reaction at fuel cell cathodes, and their activities were evaluated and compared. Note that from the experimental results presented above (Figure 4) it is likely that Au was deposited onto the Ag surface in the form of nanoscale clusters, which are anticipated to exhibit interesting (electro)catalytic activity, as evidenced in a series of previous studies.[26] Experimentally, the AgC6 and AgAu bimetallic nanoparticles prepared above were loaded onto the glassy carbon disk of a rotating ring-disk electrode. The electrodes were first subject to repeated potential cycling within the potential range of +0.2 to +1.0 V in a nitrogen-saturated 0.1 M NaOH solution at a potential sweep rate of 100 mV/s, until steady voltammograms appeared, so as to expose part of the nanoparticle surfaces for electrocatalytic reactions. The assessments of their electrocatalytic activities were then carried out in an oxygen-saturated 0.1 M NaOH solution.

Figure 6 depicts the RRDE voltammograms of the glassy-carbon disk electrode modified with a calculated amount of (a) AgC6, (b) bulk-exchange and (c) Janus nanoparticles in an oxygen-saturated 0.1 M NaOH solution at varied electrode rotation rates (from 400 to 2500 rpm). It can be seen that in all cases, at the disk electrode (solid curves) apparent cathodic currents started to emerge at potentials more negative than about ca. +0.8 V and reached a (quasi-)plateau at potentials more negative than +0.6 V. These observations were ascribed to the electroreduction of oxygen catalyzed by the respective nanoparticle catalysts. Note that the behaviors were rather consistent with those reported in the literature for Ag nanoparticles and single crystal electrodes,[27] indicating the apparent ORR activity of the nanoparticles despite their organic capping layers. A more careful analysis shows that the onset potential of the oxygen reduction reactions actually varied with the nanoparticle catalysts, +0.792 V for the original AgC6 nanoparticles, and +0.809 V for the bulk-exchange AgAu nanoparticles, and +0.917 V for the Janus AgAu nanoparticles.

dx.doi.org/10.1021/la303513x | *Langmuir* 2012, 28, 17143−17152

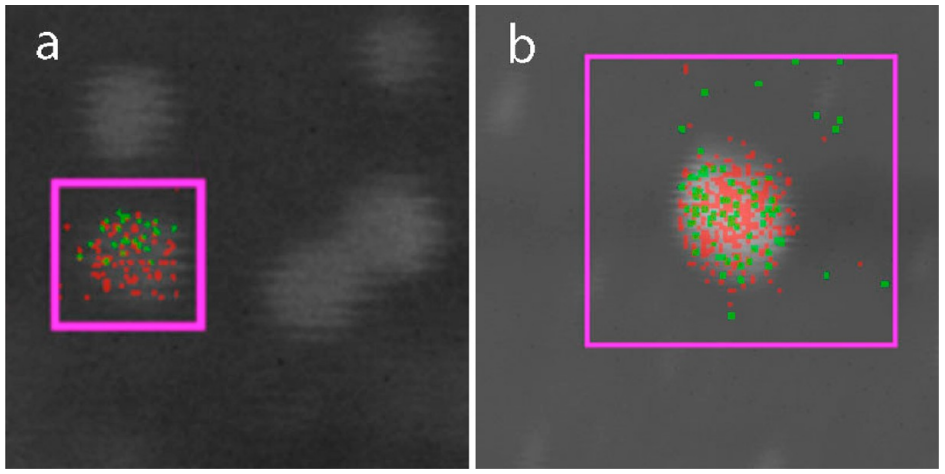

Figure 4. Representative false-color EDS elemental maps of a (a) Janus and (b) bulk-exchange nanoparticle with red symbols for Ag and green for Au. The samples are the same as those as in Figure 3.

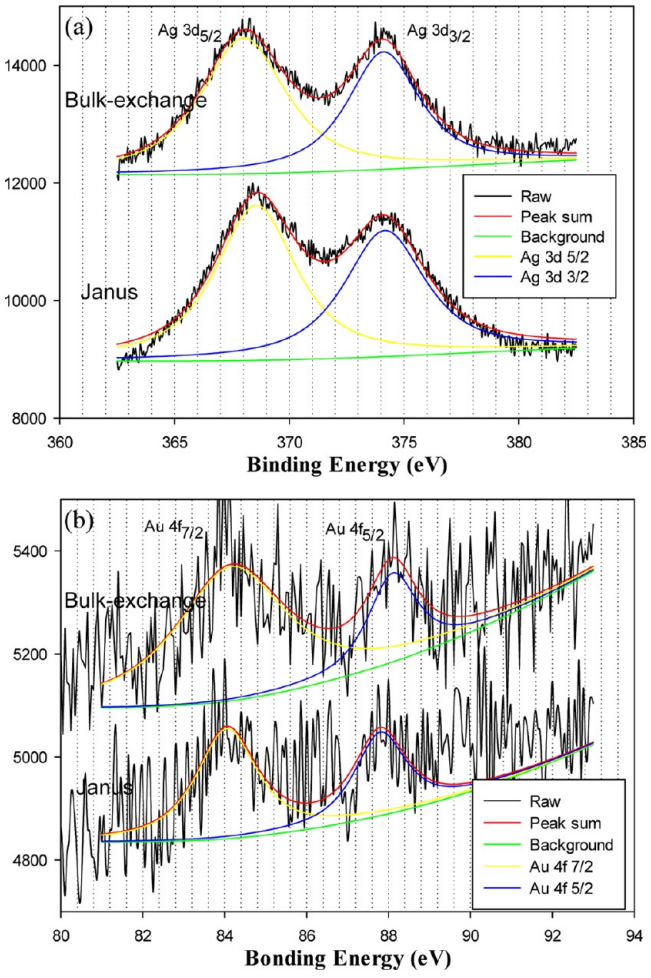

Figure 5. XPS survey spectra of (a) Ag 3d and (b) Au 4f electrons for (bottom curves) Janus and (top curves) bulk exchange nanoparticles.

This suggests that the electron-transfer kinetics of oxygen reduction was facilitated by the incorporation of a minimal amount of Au onto the Ag nanoparticle surface (Table 1), with the ORR activity increasing in the order of AgC6 < bulk-exchange < Janus AgAu nanoparticles.

In addition, the amounts of hydrogen peroxide generated during the oxygen reduction were quantified by collection

Table 1. Binding Energies of the Ag 3d and Au 4f Electrons in Bulk-Exchange and Janus AgAu Nanoparticles and Their Au/Ag Atomic Ratios by XPS Measurements

	Ag		Au		
	$3d_{5/2}$	$3d_{3/2}$	$4f_{7/2}$	$4f_{5/2}$	Au/Ag atomic ratio
bulk-exchange nanoparticles	368.00	374.10	84.20	88.15	1:16.3
Janus nanoparticles	368.55	374.20	84.05	87.85	1:21.9

experiments with the ring potential set at +1.4 V. From Figure 6, it can be seen that the ring currents (dashed curves) were all substantially smaller than those at the disk at all rotation rates, and decreased in the order of AgC6 < bulk-exchange < Janus nanoparticles. Importantly, from the ratio between the ring (I_R) and disk (I_D) currents, the number of electron transfer (n) in oxygen reduction can be estimated by $n = 4I_D/(I_D + (I_R/N))$.[14] For instance, at 2500 rpm, the n values for the three nanoparticle catalysts were estimated to be 2.46 ± 0.02 for AgC6, 3.15 ± 0.10 for the bulk-exchange, and 3.36 ± 0.03 for the Janus nanoparticles within the potential range of +0.2 to +0.6 V. This indicates that oxygen was more likely to undergo four-electron reduction to OH^- with the bimetallic AgAu nanoparticles, whereas with monometallic AgC6 the final products appeared to be dominated by hydrogen peroxide.[11b,27a,28] The latter is drastically different from the results observed in a previous study with adenosine 5′-triphosphate-(ATP)-capped Ag nanoparticles,[27a] where oxygen were found to undergo four-electron reduction. This discrepancy most probably arose from the different chemical environments on the Ag nanoparticle surfaces. In the present study, the Ag cores remained partly passivated by hydrophobic hexanethiolate ligands, even after an electrochemical activation procedure as described above. This impedes the accessibility of the Ag surface by the reaction intermediates of oxygen reduction as well as electrolyte counterions. By contrast, the hydrophilic ATP ligands might be effectively removed from the nanoparticle surface rendering it readily accessible and thus facilitating the oxygen reduction reactions.[27a]

The electron-transfer kinetics was further analyzed by the Koutecky–Levich plots (eq 1a), as the disk voltammetric currents (I_D) may involve both kinetic (I_k) and diffusion (I_d) controlled contributions

dx.doi.org/10.1021/la303513x | Langmuir 2012, 28, 17143–17152

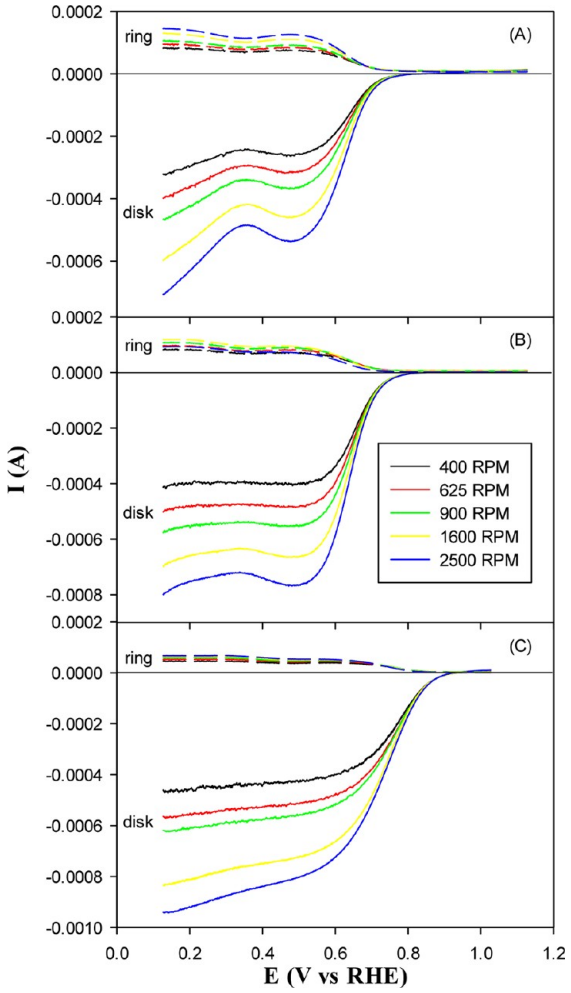

Figure 6. RRDE voltammograms of a glassy-carbon disk-gold ring electrode with the disk modified with (a) as-prepared AgC6, (b) bulk-exchange, and (c) Janus nanoparticles in an oxygen-saturated 0.1 M NaOH solution. The metal loadings were (a) 2.38, (b) 2.44, and (c) 2.60 μg, as determined by thermogravimetric analysis. Electrode potential sweep rate was 10 mV/s, the ring potential was set at +1.4 V, and rotation rates were specified in the figure legends.

$$\frac{1}{I_D} = \frac{1}{I_k} + \frac{1}{I_d} = \frac{1}{I_k} + \frac{1}{B\omega^{1/2}} \quad (1a)$$

$$B = 0.62nFAC_O{D_O}^{2/3}\nu^{-1/6} \quad (1b)$$

$$I_k = nAFkC_O \quad (1c)$$

where F is the Faradaic constant (96500 C/mol), D_O is the diffusion coefficient of O_2 in 0.1 M NaOH aqueous solution (1.93×10^{-5} cm^2/s), ν is the kinematic viscosity of the solution (1.09×10^{-2} cm^2/s), C_O is the oxygen concentration in O_2-saturated solutions (1.26×10^{-6} mol/cm^3), ω is the electrode rotation rate, k is the electron-transfer rate constant, and A is the geometric surface area of the electrode.[29] Figure 7 shows the corresponding Koutecky–Levich plots (${I_D}^{-1}$ vs $\omega^{-1/2}$) for the three nanoparticle catalysts within the potential range of +0.58 to +0.82 V where kinetic contributions were significant. It can be seen that all experimental data exhibited good linearity and the slopes were rather consistent in each nanoparticle sample within the corresponding potential range. This observation is usually taken as a strong indication of a first-order reaction with respect to dissolved O_2.

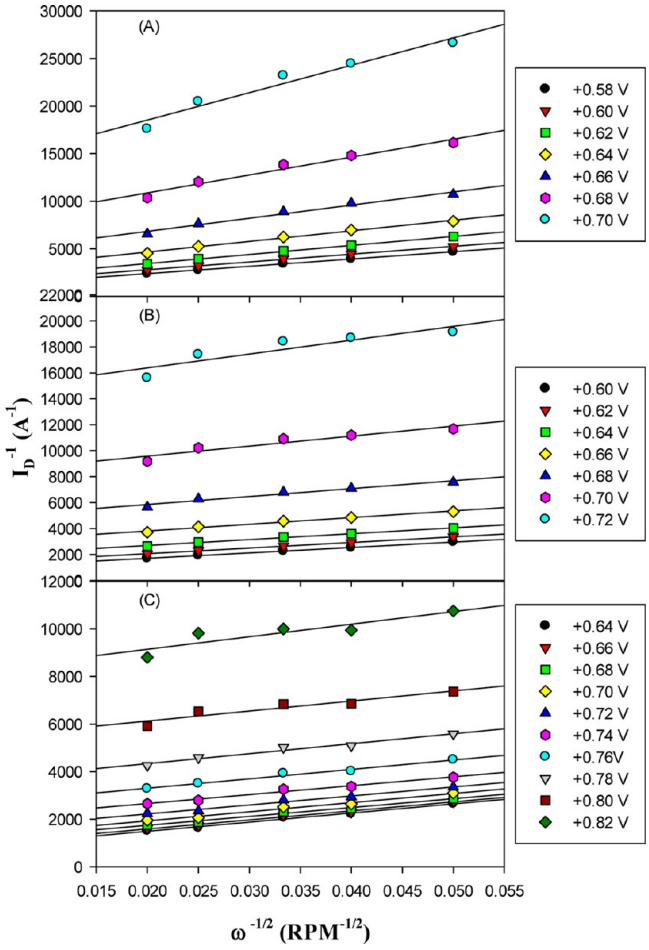

Figure 7. Koutecky–Levich plots of (a) as-prepared AgC6, (b) bulk-exchange, and (c) Janus nanoparticles in oxygen reduction in an oxygen-saturated 0.1 M NaOH solution. Symbols are experimental data acquired from Figure 6, and lines are the corresponding linear regressions.

Additionally, from the linear regressions in Figure 7, the kinetic currents (I_k) could also be estimated from the y-axis intercepts (eq 1c). This is manifested in the Tafel plot of Figure 8, where one can see that at all nanoparticle catalysts, the kinetic currents increased with increasingly negative electrode potentials, and more importantly, at all electrode potentials (from +0.58 to +0.82 V), the kinetic current increased by the order of AgC6 < bulk-exchange < Janus nanoparticles. For instance, the area-specific kinetic current density (J_s, I_k normalized by the disk geometrical area) at +0.68 V can be estimated to be 5.68 A/m^2 for AgC6, 8.75 A/m^2 for the bulk-exchange particles, and 40.64 A/m^2 for the Janus nanoparticles. It can be seen that whereas the current density of the bulk-exchange nanoparticles was only about 50% higher than that of AgC6, the activity of the Janus nanoparticles was more than seven times higher. Note that in a previous study with adenosine 5′-triphosphate capped-Ag nanoparticles (diameter 4.5 nm) or bulk polycrystalline silver,[27a] the kinetic current density at similar potentials was 30 to 50 A/m^2.

Similar behaviors can be seen with the mass-specific kinetic current density (J_m, I_k normalized by the metal loading of the corresponding nanoparticles, Figure S1 in the Supporting Information), as for practical applications, mass-specific activity is also an important parameter in the quantitative evaluation of

dx.doi.org/10.1021/la303513x | Langmuir 2012, 28, 17143–17152

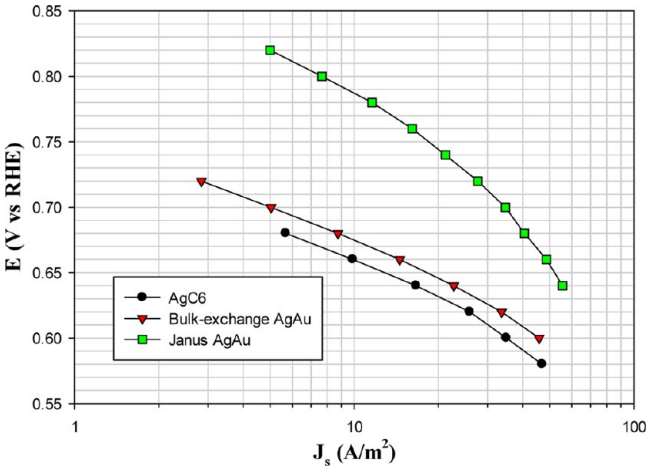

Figure 8. Tafel plots of the area-specific kinetic current densities at varied electrode potentials. Solid symbols are experimental data obtained from the *y*-axis intercepts of the linear regressions in Figure 7, and lines are for eye-guiding only.

the performance of precious metal catalysts. From Figure S1, the values of J_m at +0.68 V for the three nanoparticle catalysts can be found at 59.0 (AgC6), 88.6 (bulk-exchange nanoparticles), and 386.4 A/g (Janus nanoparticles), respectively. One can see that, in comparison with the original AgC6 nanoparticles, bulk-exchange AgAu nanoparticles again showed an activity that was 50% higher, and the Janus nanoparticles exhibited an even higher activity that was more than six times that of AgC6. This once again suggests that the Janus nanoparticles, despite a minimal loading of Au on the nanoparticle surface, represent the best catalysts within the present experimental context.

Furthermore, it can be seen from Figure 8 that the Tafel plots of the three nanoparticle catalysts exhibit two linear segments of different slopes. At low current densities (J_s < 20 A/m^2), linear regressions show that the slopes are 85.6 mV/dec for AgC6, 84.3 mV/dec for bulk-exchange nanoparticles, and 116.8 mV/dec for Janus nanoparticles; whereas at current densities >20 A/m^2, the respective slope increases to 154.0, 130.4, and 263.4 mV/dec Note that for oxygen electroreduction at nanoparticle catalyst surfaces, the Tafel slopes are typically found at 60 or 120 mV/dec, where the former corresponds to a pseudo two-electron reaction as the rate determining step and in the latter, the rate determining step is presumed to be the first-electron reduction of oxygen.[30] The results from Figure 8 suggest that the reduction mechanism is similar for the AgC6 and bulk-exchange nanoparticles where the reactions were limited largely by a pseudo two-electron reduction reaction at low current densities and at high current densities the first electron transfer of oxygen was the rate-determining step (implying that subsequent reduction and O−O bond breaking was facile). Such a behavior has been observed with a pure Pt surface.[30] By contrast, for the Janus nanoparticles, the oxygen reduction reactions were primarily determined by the first electron-transfer reaction of oxygen at low current densities; whereas at high current densities the Tafel slope (263.4 mV/dec) exhibited a rather large deviation from 120 mV/dec. Similar results were reported previously. For instance, in a previous study Ye and Crooks[31] examined the electrocatalytic activity of dendrimer-capped Pt and PtPd alloy nanoparticles in oxygen reduction and observed Tafel slopes around 160 mV/dec at high overpotentals. These observations suggest that the adsorption of oxygen and reaction intermediates played an increasingly important role in determining the electron-transfer dynamics of oxygen reduction reactions, as the kinetics of the reduction of adsorbed oxygen and cleavage of O−O bonds was enhanced at increasingly negative electrode potentials. These behaviors are consistent with the mechanism of oxygen reduction in alkaline media, as detailed below.

In previous studies of oxygen electroreduction on Ag in alkaline media,[27] the reaction mechanism was found to be similar to that on Pt. The key steps may be summarized below[32]

$$O_2 + * + e \rightarrow O_2^-* \quad (2a)$$

$$O_2^-* + H_2O \rightarrow HO_2* + OH^- \quad (2b)$$

$$HO_2* + e \rightarrow HO_2^-* \quad (2c)$$

$$HO_2^-* + H_2O + e \rightarrow OH* + 2OH^- \quad (2d)$$

$$OH* + e \rightarrow OH^- + * \quad (2e)$$

where asterisks denote surface-adsorbed species. Of these, the first-electron reduction of O_2* to HO_2* is proposed to be the rate-determining step (2a and 2b), and the subsequent reaction step (2d) involves the breaking of the O−O bond. Note that on a catalyst surface, if the adsorption of oxygen is too weak, the breaking of the O−O bond will be slow. In contrast, strong adsorption of oxygen can readily break the O−O bond, but at the expense of forming strongly bound O and OH species as a result of water oxidation.[33] The binding of oxygen on silver is considerably less strong than that on Pt, thus pure Ag is less active for O_2 reduction than Pt because the weaker Ag−$O_{2,abs}$ interaction makes the breaking of the O−O bond more difficult. Alloying with gold appeared to lead to enhanced bonding with O_2, as gold nanoparticles, in particular, subnanometer-sized gold clusters, are known to exhibit apparent activity in oxygen adsorption and subsequent electroreduction,[26a] as a result of the increasing d-band vacancy for strong metal-O_2 interactions and weakened O−O bonds.[34] Note that the Janus nanoparticles exhibited an even better performance than the bulk-exchange ones, although both showed a comparable Au coverage (Table 1). The detailed mechanism is not clear at this point, although there are several possible contributing factors such as electronically modified Au clusters, interfacial interactions between Au clusters and Ag, and spilling effects. Of these, the segregation of the hydrophilic and polar MPD ligands on the Janus nanoparticle surface might further facilitate charge transfer from Ag to Au, as evidenced in XPS measurements (Figure 5), further shifting the d-band center to the Fermi level for optimal oxygen adsorption and reduction.

Additionally, if the O and OH species produced during ORR (eqs 2a−e) are strongly adsorbed onto the catalyst surface, further reduction of O_2 may be inhibited, since the activation energies for O and OH reduction have been found to be relatively high in the low overpotential region in which fuel cell cathodes would ideally be operated.[34a] The observed enhancement of the catalytic activity of the bimetallic AgAu (either bulk exchange or Janus) nanoparticles, as compared to that of the monometal AgC6 nanoparticle, may be correlated with the weakened adsorption of oxygen species (e.g., O_{ads} and OH_{ads}) on the Ag surfaces by the Au sites, as partial electron transfer occurred from Ag to Au (e.g., Figure 5). Such a phenomenon

dx.doi.org/10.1021/la303513x | *Langmuir* 2012, 28, 17143−17152

has also been observed with other Ag-based[11] or Pt-based[35] alloys. Note that the bonding energies of O and OH on Au are in general higher than those on Ag, implying that the overall adsorption of oxygen species to form water would be facilitated on the bimetallic AgAu nanoparticles, as compared to monometallic Ag nanoparticles. That is, the incorporation of Au onto Ag nanoparticles forming surface alloys[36] favors the ORR catalytic activity.

CONCLUSION

In this present study, bimetallic AgAu Janus nanoparticles were prepared by confining the galvanic exchange reactions of AgC6 nanoparticles with the Au^{I}-MPD complex to the top face of the AgC6 nanoparticles. The asymmetrical distribution of the surface organic ligands was confirmed by contact angle measurements, whereas the bimetallic nature of the metal cores was evidenced in elemental mapping based on energy-dispersive X-ray analysis as well as XPS measurements. Despite a minimal loading of Au onto the Ag nanoparticle surface, the resulting bimetallic nanoparticles exhibited markedly enhanced electrocatalytic activity in oxygen reduction, as compared to the original monometallic Ag nanoparticles, and the electrocatalytic performance of the Janus nanoparticles was even better than that of the bulk-exchange counterparts. Notably, the area- and mass-specific current densities of the Janus nanoparticles were more than seven and six times that of the monometallic Ag nanoparticles, respectively. In the bulk-exchange nanoparticles, the two metal elements were presumably distributed evenly in the nanoparticle cores, whereas in the Janus nanoparticles, the segregated partition of polar MPD ligands from the apolar hydrophobic hexanethiolates was likely to further facilitate electron transfer from Ag to Au, leading to additional improvement of the adsorption and reduction of oxygen. These results further demonstrate the significance of interfacial engineering in nanoparticle functionalization and the impacts on their electrocatalytic activity.

ASSOCIATED CONTENT

Supporting Information

Variation of mass-specific current density with electrode potential for the three nanoparticle catalysts. This material is available free of charge via the Internet at http://pubs.acs.org.

AUTHOR INFORMATION

Notes

The authors declare no competing financial interest.

ACKNOWLEDGMENTS

This work was supported, in part, by the National Science Foundation (CHE, 1012258; DMR, 0804049; and CBET, 12158839) and the ACS Petroleum Research Fund (49137-ND10). TEM and XPS studies were carried out at the National Center for Electron Microscopy and the Molecular Foundry of the Lawrence Berkeley National Laboratory as part of a user project.

REFERENCES

(1) (a) Casagrande, C.; Veyssie, M. Janus Beads - Realization and 1 St Observation of Interfacial Properties. *CR Acad. Sci. Ser. II* **1988**, *306* (20), 1423−1425. (b) Degennes, P. G. Soft Matter. *Science* **1992**, *256* (5056), 495−497.

(2) (a) Perro, A.; Reculusa, S.; Ravaine, S.; Bourgeat-Lami, E. B.; Duguet, E. Design and synthesis of Janus micro- and nanoparticles. *J. Mater. Chem.* **2005**, *15* (35−36), 3745−3760. (b) Roh, K. H.; Martin, D. C.; Lahann, J. Biphasic Janus particles with nanoscale anisotropy. *Nat. Mater.* **2005**, *4* (10), 759−763. (c) Suzuki, D.; Kawaguchi, H. Janus particles with a functional gold surface for control of surface plasmon resonance. *Colloid Polym. Sci.* **2006**, *284* (12), 1471−1476. (d) Nie, Z. H.; Li, W.; Seo, M.; Xu, S. Q.; Kumacheva, E. Janus and ternary particles generated by microfluidic synthesis: Design, synthesis, and self-assembly. *J. Am. Chem. Soc.* **2006**, *128* (29), 9408−9412. (e) Nisisako, T.; Torii, T.; Takahashi, T.; Takizawa, Y. Synthesis of monodisperse bicolored janus particles with electrical anisotropy using a microfluidic co-flow system. *Adv. Mater.* **2006**, *18* (9), 1152−1156.

(3) (a) Pradhan, S.; Xu, L. P.; Chen, S. W. Janus nanoparticles by interfacial engineering. *Adv. Funct. Mater.* **2007**, *17* (14), 2385−2392. (b) Pradhan, S.; Brown, L.; Konopelski, J.; Chen, S. Janus nanoparticles: reaction dynamics and NOESY characterization. *J. Nanopart. Res.* **2009**, *11* (8), 1895−1903.

(4) Hostetler, M. J.; Zhong, C. J.; Yen, B. K. H.; Anderegg, J.; Gross, S. M.; Evans, N. D.; Porter, M.; Murray, R. W. Stable, monolayer-protected metal alloy clusters. *J. Am. Chem. Soc.* **1998**, *120* (36), 9396−9397.

(5) (a) Steinbruck, A.; Csaki, A.; Festag, G.; Fritzsche, W. Preparation and optical characterization of core-shell bimetal nanoparticles. *Plasmonics* **2006**, *1* (1), 79−85. (b) Mulvaney, P.; Giersig, M.; Henglein, A. Electrochemistry of multilayer colloids: preparation and absorption spectrum of gold-coated silver particles. *J. Phys. Chem.* **1993**, *97* (27), 7061−7064.

(6) (a) Hoover, N. N.; Auten, B. J.; Chandler, B. D. Tuning Supported Catalyst Reactivity with Dendrimer-Templated Pt−Cu Nanoparticles. *J. Phys. Chem. B* **2006**, *110* (17), 8606−8612. (b) Crooks, R. M.; Zhao, M.; Sun, L.; Chechik, V.; Yeung, L. K. Dendrimer-Encapsulated Metal Nanoparticles: Synthesis, Characterization, and Applications to Catalysis. *Acc. Chem. Res.* **2000**, *34* (3), 181−190.

(7) (a) Moriguchi, I.; Matsuo, K.; Sakai, M.; Hanai, K.; Teraoka, Y.; Kagawa, S. Synthesis of size-quantized metal sulfides of Pb-Cd and Zn-Cd bimetallic systems in stearate Langmuir-Blodgett films. *J. Chem. Soc., Faraday Trans.* **1998**, *94* (15), 2199−2204. (b) Shon, Y. S.; Dawson, G. B.; Porter, M.; Murray, R. W. Monolayer-protected bimetal cluster synthesis by core metal galvanic exchange reaction. *Langmuir* **2002**, *18* (10), 3880−3885. (c) Zhang, J.; Lima, F. H. B.; Shao, M. H.; Sasaki, K.; Wang, J. X.; Hanson, J.; Adzic, R. R. Platinum monolayer on nonnoble metal-noble metal core-shell nanoparticle electrocatalysts for O-2 reduction. *J. Phys. Chem. B* **2005**, *109* (48), 22701−22704. (d) Cobley, C. M.; Xia, Y. N. Engineering the properties of metal nanostructures via galvanic replacement reactions. *Mater. Sci. Eng. Res.* **2010**, *70* (3−6), 44−62.

(8) Bond, G. C. Gold: a relatively new catalyst. *Catal. Today* **2002**, *72* (1−2), 5−9.

(9) Varcoe, J. R.; Slade, R. C. T. *Fuel Cell* **2004**, 5.

(10) (a) Asazawa, K.; Yamada, K.; Tanaka, H.; Oka, A.; Taniguchi, M.; Kobayashi, T. Platinum-Free Zero-Carbon-Emission. An Easy Fuelling Direct Hydrazine Fuel Cell for Vehicles. *Angew. Chem.* **2007**, *119* (42), 8170−8173. (b) Rousseau, S.; Coutanceau, C.; Lamy, C.; Leger, J. M. Direct ethanol fuel cell (DEFC): Electrical performances and reaction products distribution under operating conditions with different platinum-based anodes. *J. Power Sources* **2006**, *158* (1), 18−24.

(11) (a) Fernández, J. L.; Walsh, D. A.; Bard, A. J. Thermodynamic Guidelines for the Design of Bimetallic Catalysts for Oxygen Electroreduction and Rapid Screening by Scanning Electrochemical Microscopy. M−Co (M: Pd, Ag, Au). *J. Am. Chem. Soc.* **2004**, *127* (1), 357−365. (b) Hu, F.-P.; Zhang, X.-G.; Xiao, F.; Zhang, J.-L. Oxygen reduction on Ag−MnO2/SWNT and Ag−MnO2/AB electrodes. *Carbon* **2005**, *43* (14), 2931−2936.

(12) Brauer, G. *Handbook of preparative inorganic chemistry*, 2nd ed.; Academic Press: New York, 1963.

(13) Brust, M.; Walker, M.; Bethell, D.; Schiffrin, D. J.; Whyman, R. Synthesis of Thiol-Derivatized Gold Nanoparticles in a 2-Phase

Liquid-Liquid System. *J. Chem. Soc., Chem. Commun.* **1994**, *7*, 801−802.
(14) Zhou, Z. Y.; Kang, X. W.; Song, Y.; Chen, S. W. Enhancement of the electrocatalytic activity of Pt nanoparticles in oxygen reduction by chlorophenyl functionalization. *Chem. Commun.* **2012**, *48* (28), 3391−3393.
(15) Gloaguen, F.; Andolfatto, F.; Durand, R.; Ozil, P. Kinetic study of electrochemical reactions at catalyst-recast ionomer interfaces from thin active layer modelling. *J. Appl. Electrochem.* **1994**, *24* (9), 863−869.
(16) Creighton, J. A.; Eadon, D. G. Ultraviolet Visible Absorption-Spectra of the Colloidal Metallic Elements. *J. Chem. Soc., Faraday Trans.* **1991**, *87* (24), 3881−3891.
(17) Hsu, S.-W.; On, K.; Gao, B.; Tao, A. R. Polyelectrolyte-Templated Synthesis of Bimetallic Nanoparticles. *Langmuir* **2011**, *27* (13), 8494−8499.
(18) Link, S.; Wang, Z. L.; El-Sayed, M. A. Alloy formation of gold-silver nanoparticles and the dependence of the plasmon absorption on their composition. *J. Phys. Chem. B* **1999**, *103* (18), 3529−3533.
(19) (a) Laibinis, P. E.; Fox, M. A.; Folkers, J. P.; Whitesides, G. M. Comparisons of Self-Assembled Monolayers on Silver and Gold - Mixed Monolayers Derived from $HS(CH_2)_{21}X$ and $HS(CH_2)_{10}Y$ (X, Y = CH_3, CH_2OH) Have Similar Properties. *Langmuir* **1991**, *7* (12), 3167−3173. (b) Tao, Y. T.; Lee, M. T. Control of Molecular Chain Tilt in Self-Assembled Monolayers and Its Effect on Wetting Properties. *Thin Solid Films* **1994**, *244* (1−2), 810−814.
(20) Song, Y.; Klivansky, L. M.; Liu, Y.; Chen, S. Enhanced Stability of Janus Nanoparticles by Covalent Cross-Linking of Surface Ligands. *Langmuir* **2011**, *27* (23), 14581−14588.
(21) Tian, J. Q.; Liu, S.; Zhang, Y. W.; Li, H. Y.; Wang, L.; Luo, Y. L.; Asiri, A. M.; Al-Youbi, A. O.; Sun, X. P. Environmentally Friendly, One-Pot Synthesis of Ag Nanoparticle-Decorated Reduced Graphene Oxide Composites and Their Application to Photocurrent Generation. *Inorg. Chem.* **2012**, *51* (8), 4742−4746.
(22) Chen, Y.; Goldman, A. M., Formation of one-dimensional nanoparticle chains. *Appl. Phys. Lett.* **2007**, *91* (6).
(23) Uppal, M. A.; Ewing, M. B.; Parkin, I. P. One-Pot Synthesis of Core-Shell Silver-Gold Nanoparticle Solutions and Their Interaction with Methylene Blue Dye. *Eur. J. Inorg. Chem.* **2011**, *29*, 4534−4544.
(24) Hostetler, M. J.; Wingate, J. E.; Zhong, C. J.; Harris, J. E.; Vachet, R. W.; Clark, M. R.; Londono, J. D.; Green, S. J.; Stokes, J. J.; Wignall, G. D.; Glish, G. L.; Porter, M. D.; Evans, N. D.; Murray, R. W. Alkanethiolate gold cluster molecules with core diameters from 1.5 to 5.2 nm: Core and monolayer properties as a function of core size. *Langmuir* **1998**, *14* (1), 17−30.
(25) Gupta, P.; Ulman, A.; Fanfan, S.; Korniakov, A.; Loos, K. Mixed self-assembled monolayers of alkanethiolates on ultrasmooth gold do not exhibit contact-angle hysteresis. *J. Am. Chem. Soc.* **2005**, *127* (1), 4−5.
(26) (a) Chen, W.; Chen, S. W. Oxygen Electroreduction Catalyzed by Gold Nanoclusters: Strong Core Size Effects. *Angew. Chem. Int. Ed.* **2009**, *48* (24), 4386−4389. (b) Herzing, A. A.; Kiely, C. J.; Carley, A. F.; Landon, P.; Hutchings, G. J. Identification of active gold nanoclusters on iron oxide supports for CO oxidation. *Science* **2008**, *321* (5894), 1331−1335.
(27) (a) Singh, P.; Buttry, D. A. Comparison of Oxygen Reduction Reaction at Silver Nanoparticles and Polycrystalline Silver Electrodes in Alkaline Solution. *J. Phys. Chem. C* **2012**, *116* (19), 10656−10663. (b) Blizanac, B. B.; Ross, P. N.; Markovic, N. M. Oxygen reduction on silver low-index single-crystal surfaces in alkaline solution: Rotating ring Disk(Ag(hkl)) studies. *J. Phys. Chem. B* **2006**, *110* (10), 4735−4741.
(28) (a) Meng, H.; Shen, P. K. Novel Pt-free catalyst for oxygen electroreduction. *Electrochem. Commun.* **2006**, *8* (4), 588−594. (b) Chatenet, M.; Genies-Bultel, L.; Aurousseau, M.; Durand, R.; Andolfatto, F. Oxygen reduction on silver catalysts in solutions containing various concentrations of sodium hydroxide − comparison with platinum. *J. Appl. Electrochem.* **2002**, *32* (10), 1131−1140. (c) Blizanac, B. B.; Ross, P. N.; Markovic, N. M. Oxygen electroreduction on Ag(111): The pH effect. *Electrochim. Acta* **2007**, *52* (6), 2264−2271. (d) Kim, J.; Gewirth, A. A. Mechanism of Oxygen Electroreduction on Gold Surfaces in Basic Media. *J. Phys. Chem. B* **2006**, *110* (6), 2565−2571.
(29) (a) Schumpe, A.; Adler, I.; Deckwer, W. D. Solubility of Oxygen in Electrolyte-Solutions. *Biotechnol. Bioeng.* **1978**, *20* (1), 145−150. (b) Anastasijevic, N. A.; Dimitrijevic, Z. M.; Adzic, R. R. Oxygen Reduction on a Ruthenium Electrode in Acid Electrolytes. *Electrochim. Acta* **1986**, *31* (9), 1125−1130. (c) Markovic, N. M.; Gasteiger, H. A.; Grgur, B. N.; Ross, P. N. Oxygen reduction reaction on Pt(111): effects of bromide. *J. Electroanal. Chem.* **1999**, *467* (1−2), 157−163.
(30) Zhang, J. *PEM fuel cell electrocatalysts and catalyst layers: fundamentals and applications*; Springer: London, 2008.
(31) Ye, H. C.; Crooks, R. M. Effect of elemental composition of PtPd bimetallic nanoparticles containing an average of 180 atoms on the kinetics of the electrochemical oxygen reduction reaction. *J. Am. Chem. Soc.* **2007**, *129* (12), 3627−3633.
(32) (a) Lipkowski, J.; Ross, P. N. *Electrocatalysis*; Wiley-VCH: New York, 1998. (b) Ramaswamy, N.; Mukerjee, S. Fundamental Mechanistic Understanding of Electrocatalysis of Oxygen Reduction on Pt and Non-Pt Surfaces: Acid versus Alkaline Media. *Adv. Phys. Chem.* **2012**, *2012*, 1−17.
(33) Anderson, A. B. O2 reduction and CO oxidation at the Pt-electrolyte interface. The role of H2O and OH adsorption bond strengths. *Electrochim. Acta* **2002**, *47* (22−23), 3759−3763.
(34) (a) Norskov, J. K.; Rossmeisl, J.; Logadottir, A.; Lindqvist, L.; Kitchin, J. R.; Bligaard, T.; Jonsson, H. Origin of the overpotential for oxygen reduction at a fuel-cell cathode. *J. Phys. Chem. B* **2004**, *108* (46), 17886−17892. (b) Stassi, A.; D'urso, C.; Baglio, V.; Di Blasi, A.; Antonucci, V.; Arico, A. S.; Castro Luna, A. M.; Bonesi, A.; Triaca, W. E. Electrocatalytic behaviour for oxygen reduction reaction of small nanostructured crystalline bimetallic Pt−M supported catalysts. *J. Appl. Electrochem.* **2006**, *36* (10), 1143−1149.
(35) (a) Stamenkovic, V. R.; Fowler, B.; Mun, B. S.; Wang, G. F.; Ross, P. N.; Lucas, C. A.; Markovic, N. M. Improved oxygen reduction activity on Pt3Ni(111) via increased surface site availability. *Science* **2007**, *315* (5811), 493−497. (b) Wang, C.; Markovic, N. M.; Stamenkovic, V. R. Advanced Platinum Alloy Electrocatalysts for the Oxygen Reduction Reaction. *ACS Catal.* **2012**, *2* (5), 891−898.
(36) (a) Greeley, J.; Mavrikakis, M. Alloy catalysts designed from first principles. *Nat. Mater.* **2004**, *3* (11), 810−815. (b) Zhang, J.; Vukmirovic, M. B.; Sasaki, K.; Uribe, F.; Adzic, R. R. Platinum monolayer electro catalysts for oxygen reduction: effect of substrates, and long-term stability. *J. Serb. Chem. Soc.* **2005**, *70* (3), 513−525. (c) Greeley, J.; Mavrikakis, M. Surface and subsurface hydrogen: Adsorption properties on transition metals and near-surface alloys. *J. Phys. Chem. B* **2005**, *109* (8), 3460−3471. (d) Greeley, J.; Mavrikakis, M. Near-surface alloys for hydrogen fuel cell applications. *Catal. Today* **2006**, *111* (1−2), 52−58.